

Article

Spatial and Temporal Characteristics and Mechanisms of Marine Heatwaves in the Changjiang River Estuary and Its Surrounding Coastal Regions

Minghong Xie ¹, Qiyang Ji ^{1,*}, Qingdan Zheng ², Ziyin Meng ¹, Yuting Wang ¹ and Meiling Gao ¹

¹ Marine Science and Technology College, Zhejiang Ocean University, Zhoushan 316022, China; xieminghong@zjou.edu.cn (M.X.); mengziyin@zjou.edu.cn (Z.M.); wangyuting@zjou.edu.cn (Y.W.); gaomeiling@zjou.edu.cn (M.G.)

² College of Oceanography and Ecological Science, Shanghai Ocean University, Shanghai 201306, China; m220200682@st.shou.edu.cn

* Correspondence: jiqiyang@zjou.edu.cn; Tel.: +86-0580-2661857

Abstract: Marine heatwave (MHW) events have significant consequences for marine ecosystems and human society. This paper investigates a MHW's spatial-temporal characteristics in the Changjiang River Estuary and its surrounding coastal regions (CRESs), as well as analyzes the drivers, using satellite and reanalysis data spanning from 1982–2021. The findings show that, during the last 40 years, all four of the MHW indicators have increased. The summer MHW is more severe than other seasons, showing a rising pattern from southeast to northwest. The rise of MHWs can be attributed to the increase in sea surface heat flux, weak wind speed, and powerful El Niño events. Additionally, two special MHW events were detected during the entire study period: Event A lasted for 191 days from 9 October 2006 to 17 April 2007; Event B had an average intensity of 4.93 °C from 5 July 1994 to 1 August 1994. For locations so close to each other, the characteristics of MHWs can also vary, and the mechanisms behind them are highly complex.

Keywords: MHW; sea surface temperature; the Changjiang river estuary and its surrounding coastal regions; heat flux



Citation: Xie, M.; Ji, Q.; Zheng, Q.; Meng, Z.; Wang, Y.; Gao, M. Spatial and Temporal Characteristics and Mechanisms of Marine Heatwaves in the Changjiang River Estuary and Its Surrounding Coastal Regions. *J. Mar. Sci. Eng.* **2024**, *12*, 653. <https://doi.org/10.3390/jmse12040653>

Academic Editor: Christos Stefanakos

Received: 19 March 2024

Revised: 9 April 2024

Accepted: 12 April 2024

Published: 15 April 2024



Copyright: © 2024 by the authors. Licensee MDPI, Basel, Switzerland. This article is an open access article distributed under the terms and conditions of the Creative Commons Attribution (CC BY) license (<https://creativecommons.org/licenses/by/4.0/>).

1. Introduction

Marine heatwaves are severe climate phenomena in the ocean, typically defined as occurrences where the SST surpasses a relative threshold for a duration of five days or more, covering a range of up to several thousand kilometers [1]. MHWs pose a serious threat to human survival and marine ecosystems, caused by a blend of atmospheric and oceanic mechanisms [2–8]. The MHW event in 2003 along the northwest Mediterranean region resulted in the loss of seagrass beds [4,9]. The 2011 marine heatwave event in Australia altered the structure and function of the coastal benthic ecosystem, resulting in a significant reduction in seaweed populations, which in turn affected the fishing industry [10,11]. The MHW occurrence in the Atlantic Ocean's northwest region during 2012 induced alterations in the structure of fish stocks. This, in turn, prompted adjustments in fishing practices, culminating in substantial economic losses for the fisheries industry [12]. During the 2015 and 2016 marine heatwave event in the Tasman Sea, located in southeast Australia, the area encountered its first instance of Pacific Oyster Mortality Syndrome outbreak. As a result, the number of juvenile oysters significantly decreased [13–16]. Due to the high frequency, high impact, and significant disaster-causing characteristics of marine heatwaves, their trends and formation mechanisms have gradually become key issues in marine research.

The mechanism for the formation of marine heatwaves is complex. Previous studies have revealed that marine heatwaves are typically a result of the interaction between the

climate system's internal unpredictability and the external forcing of the atmosphere. They are prone to appear in the Eastern Boundary Current and in oceanic areas significantly impacted by El Niño phenomena [1,15,17–21]. The 2023 Climate Change report states that substantial greenhouse gas emissions have caused global warming, which has raised surface temperatures by 1 °C between 2011 and 2020 compared to the period from 1850–1900 [22]. This warming has led to increased evaporation and a heightened occurrence of extreme weather events [23,24]. It is thought that anomalous heat convergence in the south-flowing East Australian Current (EAC) was the main cause of the marine heatwave event that struck southeast Australia's Tasman Sea in 2015 and 2016 [16]. Anomaly easterly winds have been created at low latitudes by the unusual strengthening of the subtropical high pressure that resulted from its westward extension. As a result, the summer southwesterly monsoon has weakened, which has had an impact on the central and western South China Sea upwelling. It is experiencing a severe marine heatwave during the summer due to the combination of these causes [25–27]. A marine heatwave that occurred in the summer of 2021 in East Korean Bay was mainly caused by the movement of an atmospheric high-voltage system, a net lateral heat flow, and feeble surface breezes. These factors collectively contributed to a reduction in seawater cooling [28]. Furthermore, the prevalence of marine heatwaves is influenced by upwelling, air–sea heat fluxes, Kuroshio intrusion, and the El Niño Southern Oscillation (ENSO), which may have very important ecological effects [16,29–31].

In recent years, the relatively frequent occurrence of marine heatwaves off China has attracted increasing attention [18,32,33]. Between 1960 and 2017, the sea area surrounding the Beibu Gulf experienced frequent marine heatwaves. This resulted from a confluence of regional and global climate conditions, in addition to the eastern Beibu Gulf's coral reefs degrading [34]. The Bohai and Yellow Sea regions saw an increase in the frequency of severe MHWs in 1982–2019, with the majority of the various grades of these events taking place in the summer [35]. Future marine heatwaves may become more common and prolonged if greenhouse gas emissions continue to rise in the latter part of the 21st century [30,36]. Reduced cloud cover, weaker winds, Kuroshio, and a strong El Niño phenomenon in the China margin and adjacent seas under the influence of natural and human activities, resulting in elevated sea surface temperatures, consequently giving rise to the occurrence of marine heatwaves, affecting fisheries resources and increasing the number of harmful algal blooms [37–39]. China's marginal seas boast abundant marine resources, with the establishment of 86 national-level marine pasture demonstration zones, and plans to construct an additional 178 by 2025 [38]. Research on the spatial–temporal variations, physical mechanisms, and ecological effects of MHWs in the marginal seas of China is especially important because of the possible effects these events may have on oceanic ecosystems and socio-economic growth [33,38,40,41].

In previous studies, researchers primarily relied on OISST data with coarser resolutions to describe and detect MHW events, which posed challenges in accurately identifying coastal MHW events. Furthermore, the characteristics of MHWs can vary in nearby geographical areas, resulting in complex formation mechanisms. However, the CRESs boast numerous marine ranches, aquaculture bases, and the largest fishing ground, the Zhoushan Fishing Ground. Considering the ecological impacts of MHW events, there is an urgent need to investigate the characteristics and formation mechanisms of coastal MHW events in CRESs, providing crucial insights into disaster prevention and mitigation efforts.

Therefore, this article aims to discover and analyze the variations in annual and summer MHWs in CRESs from 1982 to 2021. Furthermore, this paper also provides a brief analysis of the characteristics of two specific MHW events detected near the coast of Jiangsu, as well as the potential mechanisms responsible for these variations. From this study, we believe our research significantly contributes to filling the existing knowledge gap regarding MHW events in coastal regions, offering valuable insights into disaster prevention, ecosystem conservation, and future research endeavors.

2. Data and Methods

2.1. Study Area

The CRESs are situated in China mainland’s eastern region, and the average depth is approximately 100 m, as shown in Figure 1. The subtropical monsoon climate has an impact on the sea, which has an average temperature of 20 to 24 °C, and is also affected by ocean currents, solar radiation, runoff, and tides, which complicate the change in seawater temperature [42]. The study area had abundant fishery resources. However, the occurrence of marine heatwaves poses a threat to the marine ecosystem, resulting in alterations in marine fish catch production and community structure.

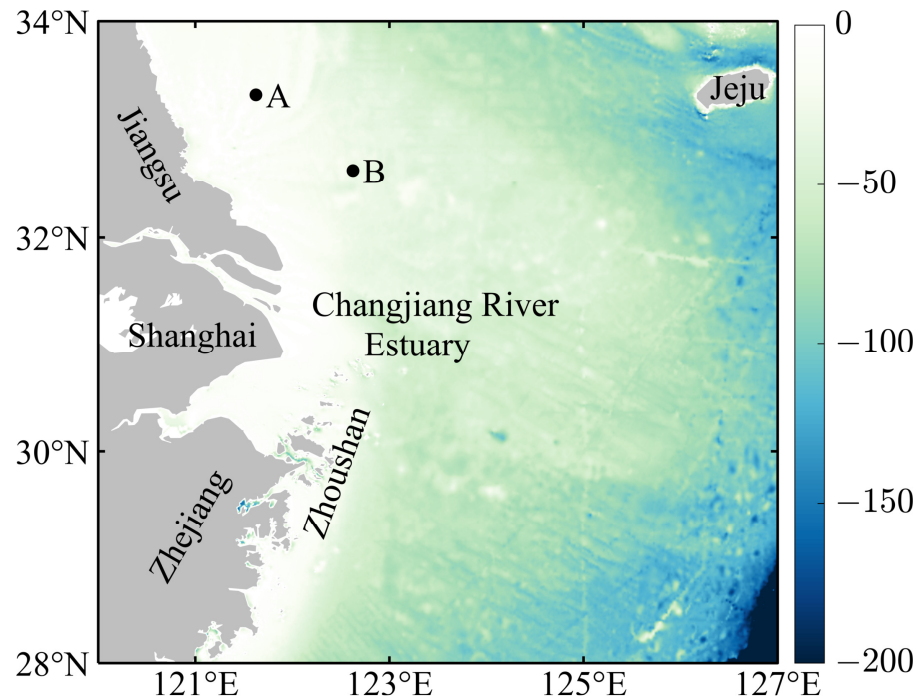


Figure 1. Bathymetry of study area (units: m); A and B are two points where typical MHWs occurred.

2.2. Data Sources

Table 1 provides all the datasets used in this paper. Operational Sea Surface Temperature and Ice Analysis (OSTIA) is daily satellite SST observation datum that is obtained from the Copernicus Marine Environmental Monitoring Service (CMEMS). It has been verified to meet the needs for precise and near real-time SST information. The Group for High-Resolution SST (GHRSSST) regional or worldwide task-sharing framework R/GTS (Regional/worldwide Task Sharing) provides satellite SST inversion data. The dataset has a horizontal resolution of 1/20° and covers the years 1982 to 2021.

Table 1. Observational and reanalysis datasets used in this study.

Dataset	Institute	Resolution	Period
OSTIA	CMEMS	0.05° × 0.05°	1982–2021 (daily)
ERA5	ECMWF	0.25° × 0.25°	1982–2021 (monthly)
ONI	NOAA	\	1994, 2006, 2007 (daily) 1982–2021 (monthly)

ERA5 represents the fifth iteration of the Global Climate Atmosphere Reanalysis System (GCRAS) developed by the European Centre for Medium-Range Weather Forecasts (ECMWF). It was created by the ECMWF’s Copernicus Climate Change Service (C3S). From 1979 to the present, it has offered hourly estimates of a broad range of atmospheric,

terrestrial, and oceanic climate variables. The variables used in this paper include monthly data for a 500 hPa geopotential height, 10 m winds, mean sea surface latent heat flux (LHF), mean sea surface sensible heat flux (SHF), mean sea surface longwave radiation (LWRF), and mean sea surface shortwave radiation (SWRF) at a resolution of 1/4° and covering the period from 1982 to 2021.

The Oceanic Niño Index (ONI) is a key indicator derived from the monitoring of ocean climate patterns by the National Oceanic and Atmospheric Administration (NOAA). This study briefly analyzes the impact of ENSO on marine heatwaves using the ONI index.

2.3. Methods

2.3.1. Define the MHW Event

An MHW is characterized as a discrete, prolonged, abnormally warm occurrence. To be more precise, it is commonly defined as a series of events in which the SST stays above the 90th percentile for a minimum of five days in a row, separated by a max. of two days [1]. Using data from an 11-day window centered on each calendar day, the 90th percentile of seasonal thresholds based on the 1982–2021 climate period was determined in this study. A summer marine heatwave is also characterized as a summer MHW that happens in June, July, and August every year.

2.3.2. Definition of MHW Indices

Based on previous studies [1,16], four indicators—HWT, HWDU, HWN, and HWI—were used in this paper to characterize MHWs in the study region. These indicators are listed in Table 2 [25,32,43]. In particular, the total days (heatwave total days, HWTs) are the sum of the MHW duration; the duration (heatwave duration, HWDU) is the consecutive period time that the temperature exceeds the threshold; the MeanInt (heatwave intensity, HWI) is the temperature deviations exceeding the threshold during its duration; the frequency (heatwave number, HWN) is the average number of discrete events occurring each year. While the number of days of MHWs increases, resulting in shorter MHWs merging into longer ones, the frequency of MHW occurrences decreases over time. This phenomenon diminishes the significance of using the frequency as a predictive indicator, as it becomes less representative of distinct MHW events. However, in contrast to previous studies, this paper still considers frequency as an indicator for analyzing the characteristics of MHWs. The scripts utilized to calculate the above metrics can be found at https://github.com/ZijieZhaoMMHW/m_mhw1.0 (accessed on 21 April 2023).

Table 2. Definitions of marine heatwave indices.

Indices	Formula	Unit
Total days	$HWT = \sum_{i=1}^N D_i$	days
Duration	$HWDU = \frac{\sum_{i=1}^N (D_i)}{N}$	days
Frequency	$HWN = N$	times
MeanInt	$HWI = \frac{\sum_i^N \sum_j^{D_i} (T_{ij} - \bar{T}_{ij})}{N}$	°C

In Table 2, N is the sum of MHWs in this particular year, and for MHW i , its duration, $\sum_{i=1}^N D_i$, is calculated as the sum duration D_i ; the variables T_{ij} and \bar{T}_{ij} are the daily surface temperature and the corresponding climatology, respectively, for day j during MHW i ; its intensity, $\sum_j^{D_i} (T_{ij} - \bar{T}_{ij})$, is calculated as the sum of the temperature deviations exceeding the threshold during its duration, D_i .

3. Results

3.1. Examples of Typical MHWs in the study areas

During the detection of MHW events throughout the entire study period in the CRESs at all grid points, two special MHW events were identified with a max. duration at point A and a max. mean intensity at point B. Table 3 shows both the MHW with maximal duration (in 2006–2007) and the MHW with maximal intensity (in 1994) for both point A and point B in parallel. As shown in Figure 2a, an MHW event with a duration of 191 days was detected from 9 October 2006 to 17 April 2007, which was the longest-duration event in the areas during the study period. Figure 2d illustrates a MHW event with the highest mean intensity of 4.93 °C, which occurred from 5 July 1994 to 1 August 1994, and had a relatively short duration. From Table 3 and Figure 2, it can be observed that the average intensities at points A and B are similar, while the duration differs significantly. We speculate that this difference arises because both points experienced relatively strong MHW events. However, at point B, the duration lower than the threshold of SST exceeds 2 days; it was divided into multiple MHW events.

Table 3. Examples of the MHW event characteristics in CRESs.

Point	MHW _{start}	MHW _{end}	Lon °E	Lat °N	Duration (Days)	MeanInt (°C)
A	09/10/2006	17/04/2007	124.225	33.375	191	1.82
B	08/10/2006	28/11/2006	124.425	32.125	52	1.62
A	01/07/1994	10/08/1994	124.225	33.375	41	3.68
B	05/07/1994	01/08/1994	124.425	32.125	28	4.93

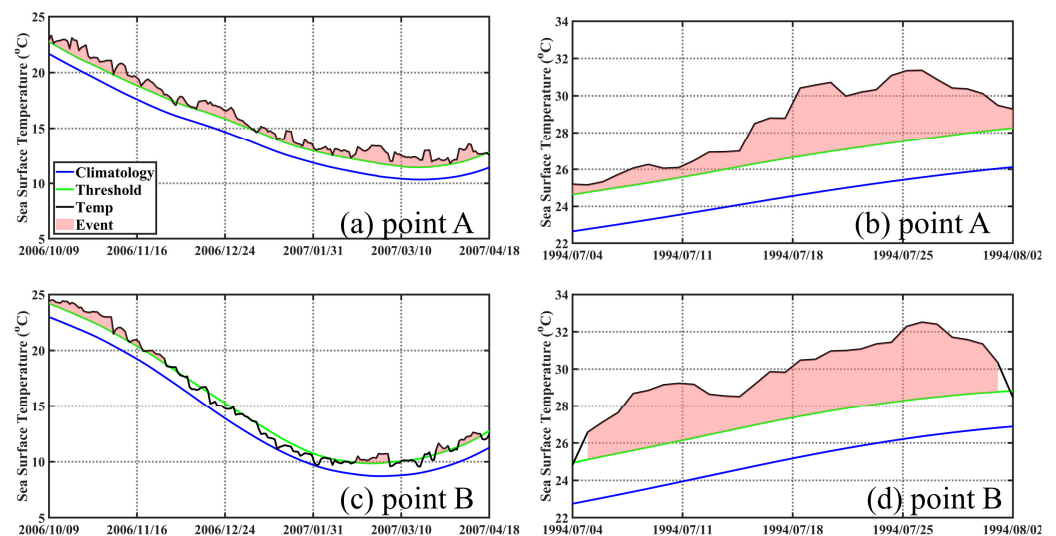


Figure 2. Examples of the MHW events at points A and B: (a) point A experiences an MHW maximum duration of 191 days in 2006–2007; (b) point A has an MHW maximum intensity of 3.68 °C in 1994; (c) point B experiences an MHW maximum duration of 52 days in 2006–2007; (d) point B has an MHW maximum intensity of 4.93 °C in 1994. The 90th percentile threshold (green), the SST time series (black), and the SST climatology (blue). The time period associated with the discovered MHW is represented by the pink-filled area.

In Table 3, MHW_{start} and MHW_{end}, respectively, represent the start date and the end date of the MHW event, with the Lon °E (longitude) and the Lat °N (latitude) occurring at point A and point B.

3.2. Characteristics of MHWs in the Study Area

3.2.1. Spatial Distribution and Trends of MHWs in 1982–2021

Figure 3 shows the main characteristics of the MHW that occurred during the study period, including the total days, duration, frequency, and the mean intensity, using a climatic base period of 1982–2021. Figure 3a shows that the coastal region of Jiangsu has the greatest annual mean total days, with more than 40 days at point A, while the annual total days in the waters west of 124° E, at the Changjiang River's mouth, and in the southern part of Jeju Island are also higher with 30–35 days, and the rest of the area with less than 30 days. Figure 3b shows that the duration of the study area is 11–13 days, with a longer duration of 13–16 days along the Jiangsu coast and Jeju Island's southern shore, and a shorter duration of about 9 days along the Zhejiang coast. Between 1982 and 2021, the study area had an average frequency of the MHW that varied between 2.5 and 3.5 times (Figure 3c). From Figure 3a–c, it can be seen that the high annual average total days of MHWs at point A and point B are mainly due to the long duration, while the high total days along the Zhejiang coast are mainly due to the high frequency of the MHWs. The annual mean intensity of MHWs generally increases northward, with an extreme point at point B, where the mean intensity is 2.4 °C, which is significantly higher than other sea areas (Figure 3d).

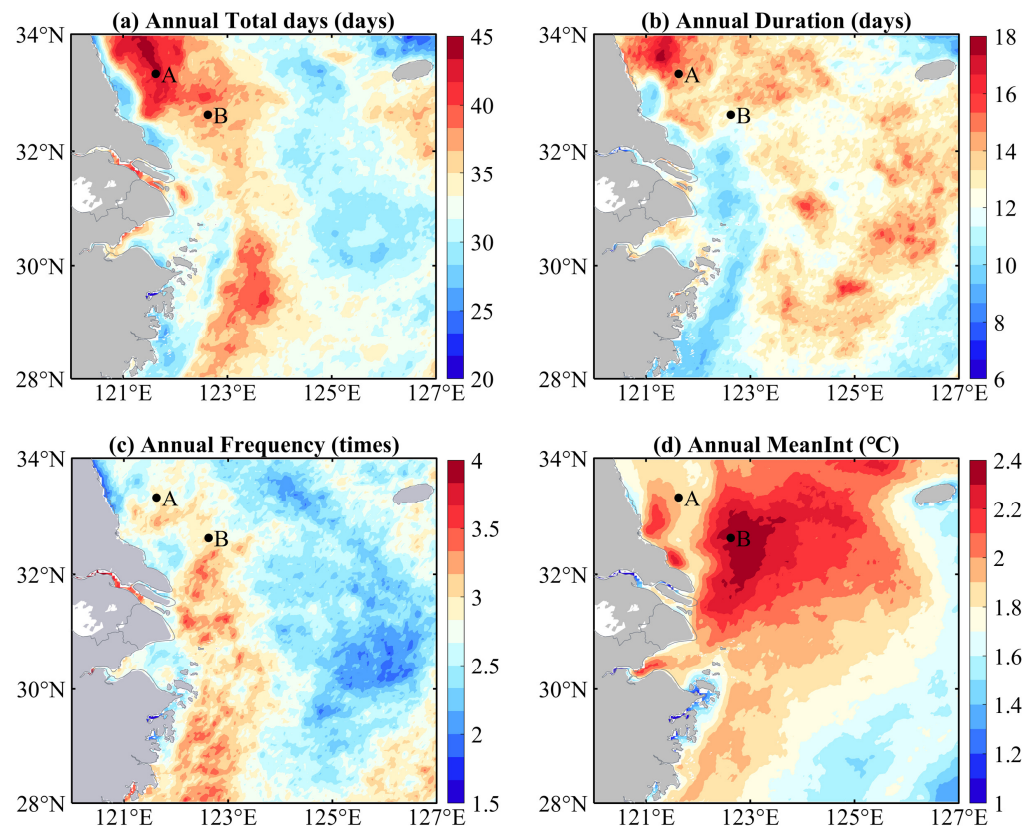


Figure 3. Spatial distributions of mean annual total days (a), duration (b), frequency (c), and mean intensity (d) of MHWs in the CRESs from 1982 to 2021. A and B are two points where typical MHWs occurred.

The spatial trend of the MHW's characteristics in the study area during 1982–2021 is shown in Figure 4, where the black markers represent passing the 99% significance test. As can be seen in Figure 4a, the trend of total days of MHWs throughout the year is statistically significant throughout the study area. The high-resolution OSTIA data solved the problem of missing values in the nearshore, and the trend values of the total days of MHWs varied between 0.5 and 4.5 days per decade, with the peak trend in total days detected along the

coast of Jiangsu Province > 4 days/decade. From Figure 4b, the trend duration of MHWs in the southern part of Jeju Island, along the coast of Jiangsu Province, and in the southern part of the Changjiang River estuary areas shows a significant increase, while the increase in the duration in the coastal areas of Zhejiang Province is not significant. The frequency and the total days of the greatest MHWs have a similar regional tendency (Figure 4a,c), and the region west of 125° E has a greater trend value of MHW frequency than the region east of 125° E. As seen in Figure 4d, the study regions have a trend of 0.01–0.02 °C/decade for mean intensity.

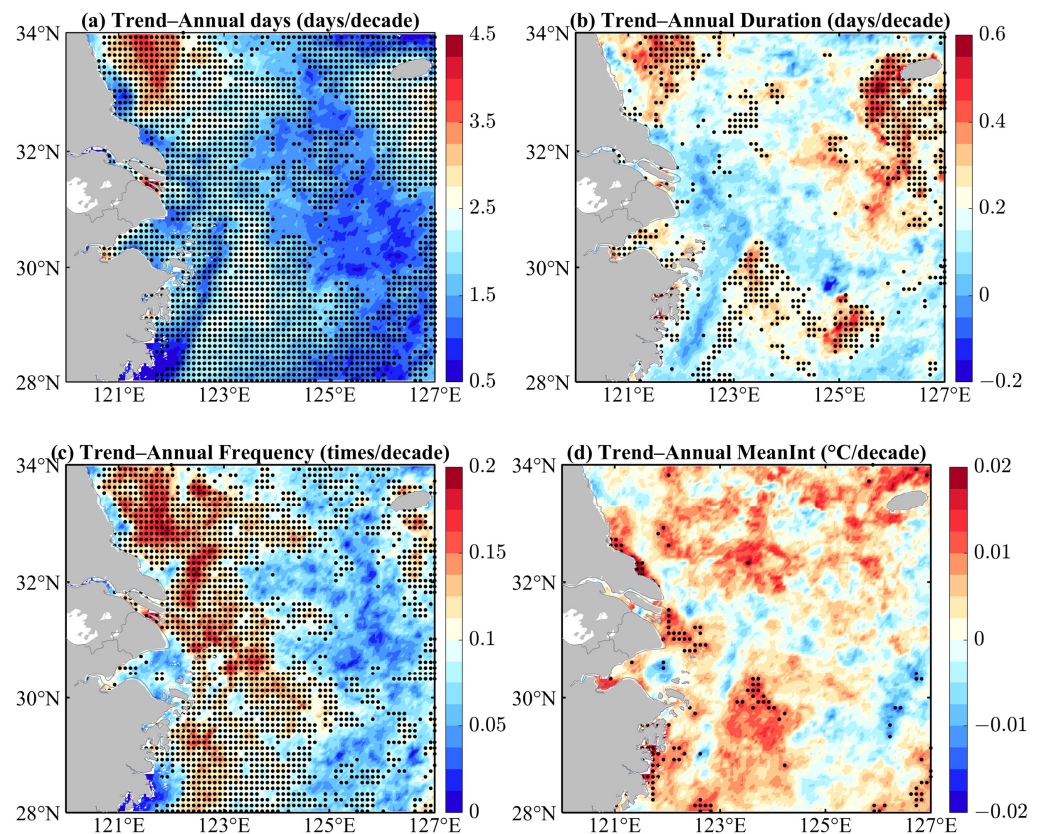


Figure 4. Trends of the MHW mean annual total days (a), duration (b), frequency (c), and mean intensity (d) of MHWs in the CRESs from 1982 to 2021. The black dot represents the 99% significance test.

3.2.2. Temporal Evolution of MHWs in 1982–2021

Figure 5 shows the temporal trends of each key index of MHWs in the study area over time throughout the study period. From Figure 5a,b, there is a rapidly increasing trend at 1.64 ± 0.28 days/decade and 0.20 ± 0.04 days/decade. At the same time, there is a similarity in the temporal characteristics of the total days and frequency; high values were observed in 1998, 2017, and 2021, especially in 2021, with the average total days of MHWs at more than 100 days, and the frequency of MHW at more than 6 times (Figure 5a,c). The mean intensity does not change significantly from 1982 to 2021 at 0.01 ± 0.01 °C/decade, as shown in Figure 5d.

To investigate the temporal characteristics of MHWs in the study area, this paper statistically examined the relationship between various key indicators of MHWs and SST in the region during 1982–2021 (Figure 6). Over the past 40 years, the annual mean SST has generally shown a clear upward trend and fitted well with the four indicators of MHWs, of which the annual mean frequency of MHWs was strongly correlated with SST ($R = 0.93$); the mean total days had the next best fit with a correlation coefficient of 0.89; the duration of MHWs with the annual mean SST was 0.78; and the mean intensity fitted relatively poorly ($R = 0.58$).

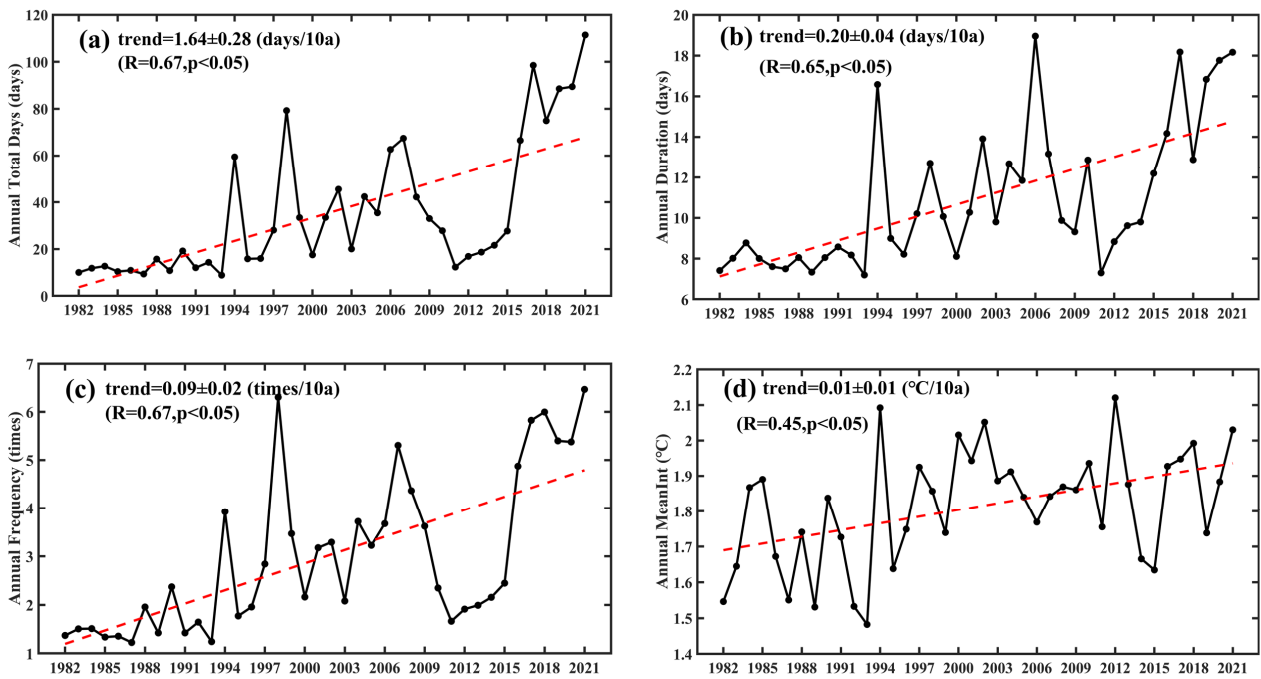


Figure 5. Temporal evolution distributions of regional average annual total days (a), duration (b), frequency (c), and mean intensity (d) of MHWs in 1982–2021 in the CRESs. The red dotted lines are linear trends.

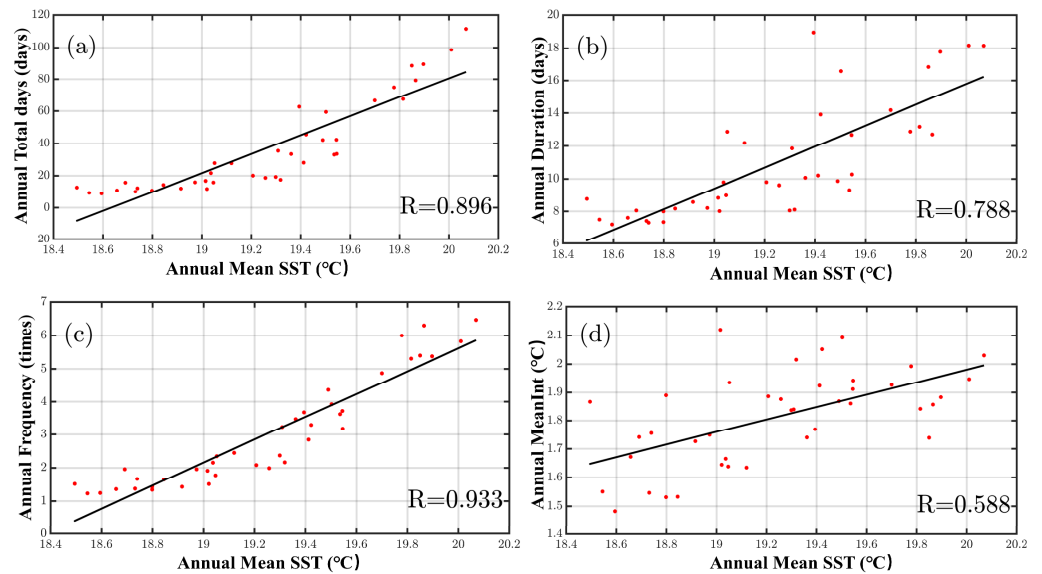


Figure 6. Scatter diagrams of mean SST and MHW mean total days (a), duration (b), frequency (c), and mean intensity (d) in the CRESs between 1982 and 2021, the best-fit linear curve being represented by the black lines.

In order to further analyze the seasonal changes in MHWs throughout the research period, the multi-year averages of the key indicators of MHWs in the four seasons during the period of 1982–2021 were counted in this paper, as depicted in Table 4 (including the uncertainty interval). As indicated in Table 4, regarding the uncertainty interval, it shows no noticeable difference among spring, autumn, and winter. Simultaneously, the average total days, duration, and mean intensity of summer MHWs surpassed those of other seasons, except for the frequency in spring, which slightly exceeded that of summer. During summer, the mean multi-annual duration of MHWs was 9.36 ± 1.19 days, the

average intensity was 1.99 ± 0.07 °C, and the average total days reached 12.48 ± 2.21 days. As a result, it is crucial to research summer MHW characteristics in the research region.

Table 4. Multi-year average of MHWs in four-season marine heatwaves in the CRESs between 1982 and 2021, including the uncertainty interval.

	Total Days (Days)	Duration (Days)	Frequency (Times)	MeanInt (°C)
Spring	12.26 ± 2.07	8.76 ± 0.85	1.35 ± 0.01	1.91 ± 0.07
Summer	12.48 ± 2.21	9.36 ± 1.19	1.32 ± 0.09	1.99 ± 0.07
Autumn	11.27 ± 1.84	9.08 ± 1.16	1.22 ± 0.08	1.60 ± 0.06
Winter	11.34 ± 1.29	8.81 ± 0.74	1.28 ± 0.05	1.49 ± 0.03

As shown in Figure 7, this paper analyzed the frequency of MHWs in four seasons over the past 40 years. After a statistical analysis, the increasing trends of MHW frequency in four seasons had no significant difference, with higher values in spring and summer. The summer frequency values in Figure 7b are high in 1994, 2001, and 2016, exceeding 1.5 °C, with a correlation coefficient of 0.55. The increasing rates of MHW frequency in autumn and winter are relatively low, which are 0.022 ± 0.006 (times/decade) and 0.015 ± 0.004 (times/decade), respectively, with a correlation coefficient of 0.51 (Figure 5c,d).

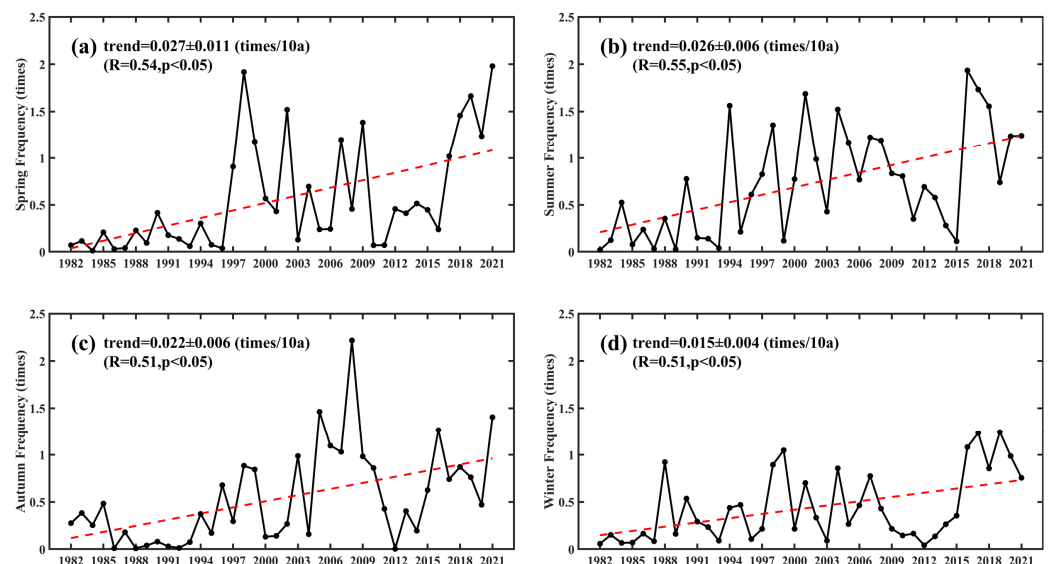


Figure 7. The year-to-year variations in the MHW frequency in the CRESs from 1982 to 2021 in spring (a), summer (b), autumn (c), and winter (d). The red dotted lines are linear trends.

3.3. Characteristics of Summer MHWs in the Study Area

3.3.1. Spatial Distribution and Trends of MHWs in Summer (1982–2021)

This paper also statistically analyzed the key indicators of the summer MHW in the CRES during 1982–2021 to better understand the MHW’s characteristics in the CRES. Figure 8a illustrates that the total days of summer MHWs are notably higher, and the two points of A and B are about 10 days, in the northern region of the CRES, in contrast to the southern sea area. In general, over a certain period of time, the longer the duration of a MHW, the less frequent its occurrences. From Figure 8b, in coastal areas (121° E– 123° E), the complexity of nearshore hydrodynamic processes contributes to the difficulty in sustaining MHW events, resulting in a shorter duration, around 8 days, but with a higher frequency. Conversely, in offshore regions (125° E– 126° E), where hydrodynamic conditions are more stable, extreme high temperatures are better sustained, resulting in a longer duration, but with less frequency, typically less than one time (Figure 8c). As evident from Figures 8d and 3d, similar to the average intensity of MHWs throughout the

year, there is also a region of high values at point B in summer, ranging from 2.5 to 3 °C, with an increasing trend towards the north. We speculate that the possible reason for this could be that point B is located in shallow waters, where it receives shortwave radiation from the sun that can heat up the seabed. In turn, the warm seabed can transfer heat to the sea surface by convection. Therefore, in the northern part of the CRES (especially at point B), the intensity of the summer MHW is higher. Conversely, in the southern part of the study area (28° N–30° N), where the depth decreases rapidly with the longitude, the intensity of MHWs also decreases rapidly with the longitude, from 2 °C to 1 °C.

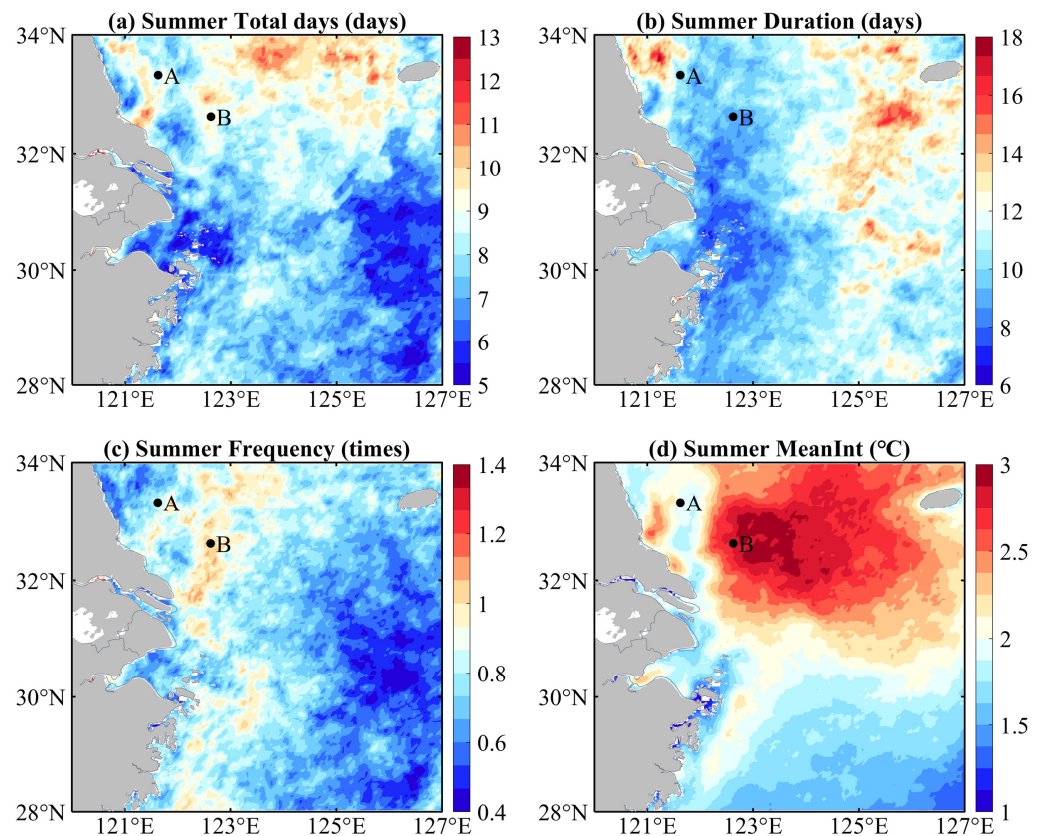


Figure 8. Spatial distributions of mean total days (a), duration (b), frequency (c), and mean intensity (d) of MHWs in the CRES from 1982 to 2021 in summer. A and B are two points where typical MHWs occurred.

Figure 9 displays the spatial trends of MHWs between 1982 and 2021 in summer, where the black markers represent passing the 95% significance test. The trend values of the total days and frequency in summer increased more along the Jiangsu coast, as shown in Figure 9a,c, but the sea area at 31° N exhibits a negative trend for both indicators. As shown in Figure 9b,d, the summer duration and mean intensity of MHWs generally do not change significantly. The majority of coastal areas experience an increase in summer duration of roughly 0.1 days per decade and a mean intensity of roughly 0.01 °C per decade. Jeju Island’s south experiences the fastest linear increase in duration and a larger increase in mean intensity occurring along the east coast of Shanghai.

3.3.2. Temporal Evolution of MHWs in Summer (1982–2021)

The features of the summer MHW during the research period were examined in this paper on a temporal scale, and this can be seen in Figure 10. The various indices of the MHW show a fluctuating trend. And there is no obvious trend of growth in the key indices of the MHW at 0.23 ± 0.09 days/decade in summer total days and at 0.08 ± 0.05 days/decade in summer duration (Figure 10a,b). As seen in Figure 10c, the average frequency of the

summer MHW peaks at 2–2.2 times in 2001, 2017, and 2018, while the average frequency is around 1.4 times in the other years, and the trends in average intensity and the average frequency are similar, at around 2 °C, as shown in Figure 10d.

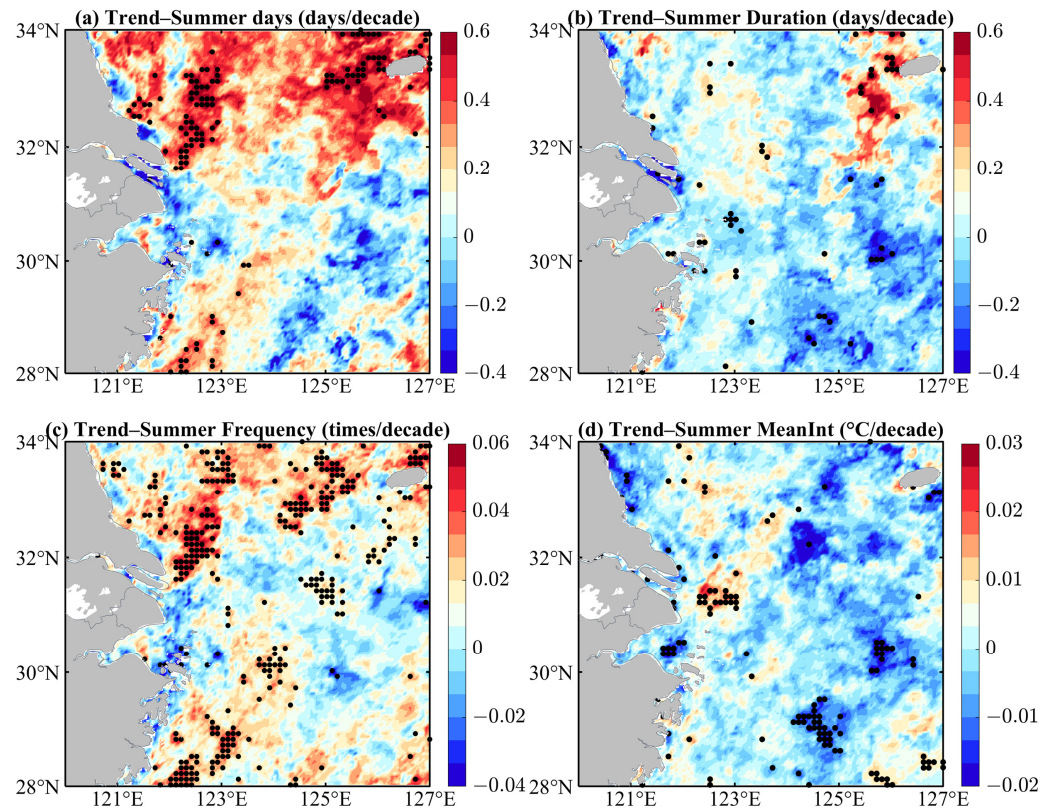


Figure 9. Trends of MHW mean total days (a), duration (b), frequency (c), and mean intensity (d) in the CRES in summer from 1982 to 2021. The black dot represents the 95% significance test.

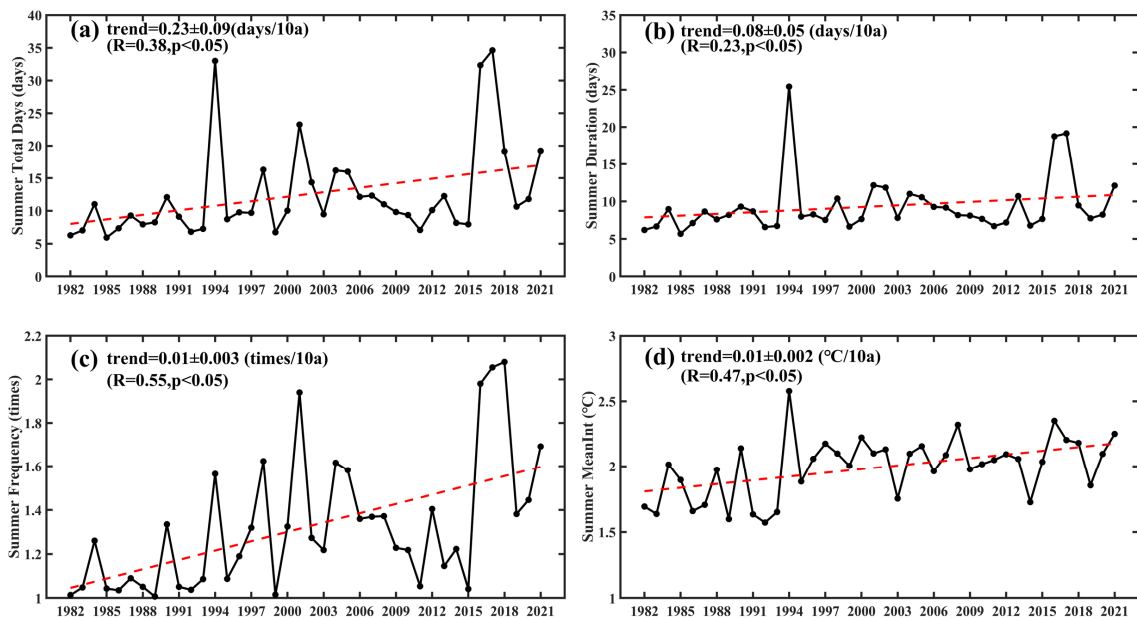


Figure 10. Temporal evolution distributions of regional average summer total days (a), duration (b), frequency (c), and mean intensity (d) of MHWs in the CRES from 1982 to 2021 in summer. The red dotted lines are linear trends.

In this paper, the relationship between various indicators of MHWs and summer SST in the study area during the summer of 1982–2021 is statistically presented in Figure 11. It is evident that the mean summer SST and the four indices of MHWs have strong correlations during the study period, among which the frequency of summer MHWs fits better with the mean summer SST ($R = 0.86$); the total days and mean summer SST have a 0.82 correlation coefficient; the mean intensity and the mean summer SST are 0.77; and the duration and mean summer SST had a relatively poor correlation ($R = 0.70$). Comparing Figure 6, the summer and annual MHW metrics show a strong correlation with the SST.

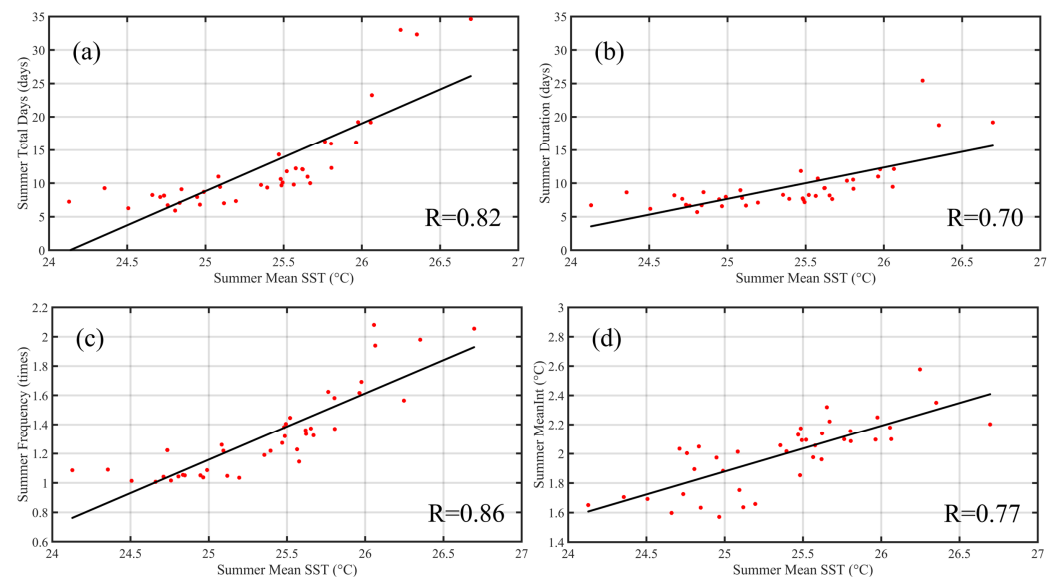


Figure 11. Scatter plots of summer mean SST and MHW mean summer total days (a), duration (b), frequency (c), and mean intensity (d) in the CRES from 1982 to 2021 in summer, the best-fit linear curve being represented by the black lines.

4. Discussion

The formation mechanism of specific MHWs in a particular area, as traditionally believed in previous studies, is generally considered to be the result of the interaction between local marine and atmospheric conditions, large-scale climate patterns, and human activities, making the formation mechanism relatively complex [44]. This paper conducted a characteristic analysis of MHWs in the CRES during 1982–2021, showing that summer MHWs are significantly more intense than in other seasons. Therefore, this paper briefly analyzed the physical mechanisms behind the summer MHWs and two special MHW events in the study area, with a focus on aspects such as sea surface heat flux, wind and the El Niño event.

4.1. Influence of Sea Surface Heat Flux

The mid-latitude atmospheric circulation can influence the heat flux at the interface between the atmosphere and ocean, thereby affecting the SST and making MHWs more likely to occur [45]. The examination of the Changjiang River Estuary's seasonal change in MHWs throughout the preceding 40 years, as well as the coastal regions surrounding it, reveals that, except for a slightly lower frequency in summer compared to spring, the other three indices are significantly higher than those of other seasons. In order to uncover the possible reasons for this phenomenon, this paper conducted a comprehensive analysis, examining the multi-year summer means, the 500 hPa geopotential heights, and the spatial distributions of SWRF, LWRF, LHF, and SHF.

This study presents spatial distribution maps depicting the 500 hPa geopotential height for the summer averages from 1982 to 2021, as shown in Figure 12. It is clear from these maps that the study area is dominantly by the subtropical high-voltage system. The

high-voltage system represents a relatively stable weather pattern, typically associated with descending air, which leads to the heating of the air and suppresses cloud formation. As a result, the weather becomes clear and dry, which makes it more likely that MHWs will occur.

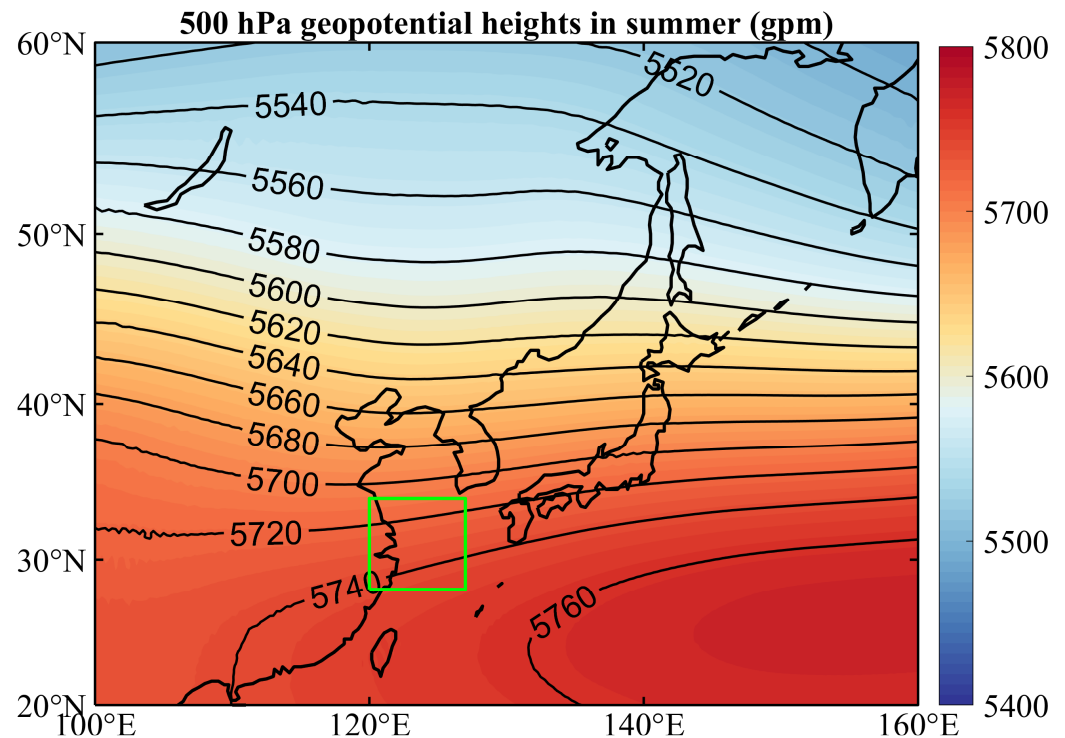


Figure 12. The 500 hPa geopotential heights during the summer averages from 1982 to 2021 in the CRES (green box).

The sea surface heat flux affects the SST, thereby leading to the occurrence of MHWs. The time-series graphs of four radiation fluxes and their sum (the sea surface heat flux) from 1982 to 2021 in summer are shown in Figure 13. In this study, the sum of the SWRF, the LWRF, the SHF, and the LHF was considered as the sea surface heat flux. The SWRF is a primary energy source for SST. As it originates from the sun and provides energy to the ocean surface upon reaching it, it leads to an increase in SST as the ocean absorbs this radiation. The LWRF is emitted by the sea surface and is primarily dependent on the SST. It plays a crucial role in dissipating excess heat from the ocean surface. The SHF represents the exchange of heat between the sea surface and the atmosphere through convection and turbulent transfer. When the SST is higher than the air temperature, the sea surface releases sensible heat, causing the SST to decrease. When seawater evaporates, the LHF occurs as water evaporates from the sea surface, releasing latent heat into the atmosphere. This process contributes to a decrease in the SST, as some of the energy is converted into latent heat during evaporation. From Figure 13, it can be observed that the SWRF plays a significant role in magnitude, ranging from 180 W/m^2 to 220 W/m^2 , followed by the LWRF and the LHF at approximately -60 W/m^2 , with the SHF having the smallest relative impact at around -3 W/m^2 . From Figure 13e, it is evident that, during the summer months from 1982 to 2021, the sea surface heat flux ranges from 100 to 110 W/m^2 , with a trend value of $-0.34 \pm 0.13 \text{ W/m}^2/\text{decade}$. The absorption of more energy leads to an increase in SST, potentially resulting in the occurrence of MHWs.

Based on the spatial distribution maps of the four radiation fluxes during the average summer conditions of the last 40 years (Figure 14), it can be observed that events with an average summer MHW of more than $2 \text{ }^\circ\text{C}$ (indicated by red markers) occur predominantly in regions with a high concentration of SWRF and comparatively low levels of LWRF,

LHF, and SHF. Specifically, Figure 14a shows a significant amount of shortwave radiation, averaging around 200 W/m^2 during the summer from 1982 to 2021. As a result, the sea surface absorbs more solar energy, creating a heating effect that influences the variation in SST. Further analysis of Figure 14b–d shows that, in the northwestern part of the area, the values of LWRF, LHF, and SHF are relatively small, which coincides with a higher intensity of MHWs in summer. This suggests that this particular marine region emits less energy to the atmosphere and outer space and there is less heat loss from the sea surface. The incidence of MHWs in this region might be attributed in part to this decreased heat loss. In summary, these observations show a correlation between summer MHWs and various radiation fluxes. They offer insightful information about the processes that lead to the development of MHWs.

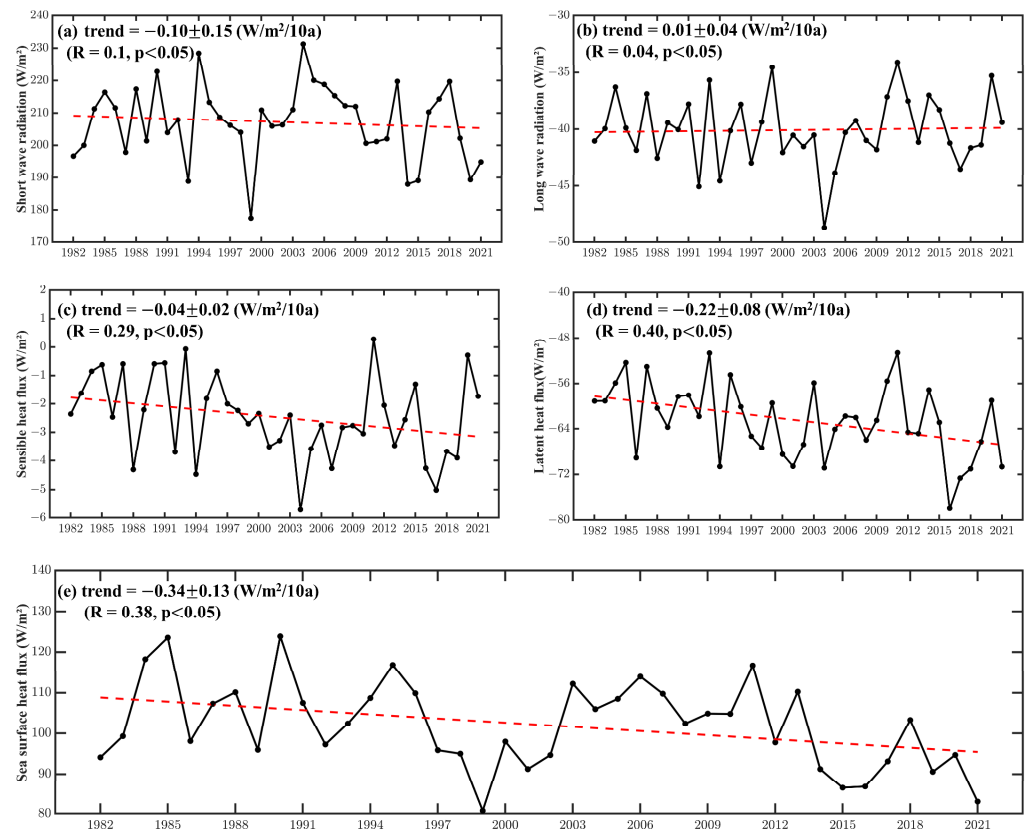


Figure 13. Temporal evolution distributions of the SWRF (a), the LWRF (b), the SHF (c), the LHF (d), and the sea surface heat flux (e) in the CRES from 1982 to 2021 in summer. The red dotted lines are linear trends.

From the observation of Figure 14a, it is clear that there is no strong correspondence between the multi-year summer mean shortwave radiation and the intensity of MHWs in summer. We speculate that this inconsistency may be due to a lagged relationship between shortwave radiation and SST. For the years 1982–2021, we thus created a graphic of the monthly mean SST and four radiation fluxes, as seen in Figure 15. The graph clearly shows that the SST peaks in August, while shortwave radiation peaks in July. Longwave radiation, sensible radiation, as well as latent heat radiation also show similar characteristics. Even during the period of maximum shortwave radiation, the relatively large specific heat capacity of seawater requires some time to absorb and store this energy. This results in a delayed response of the SST and consequently affects the MHW’s response time.

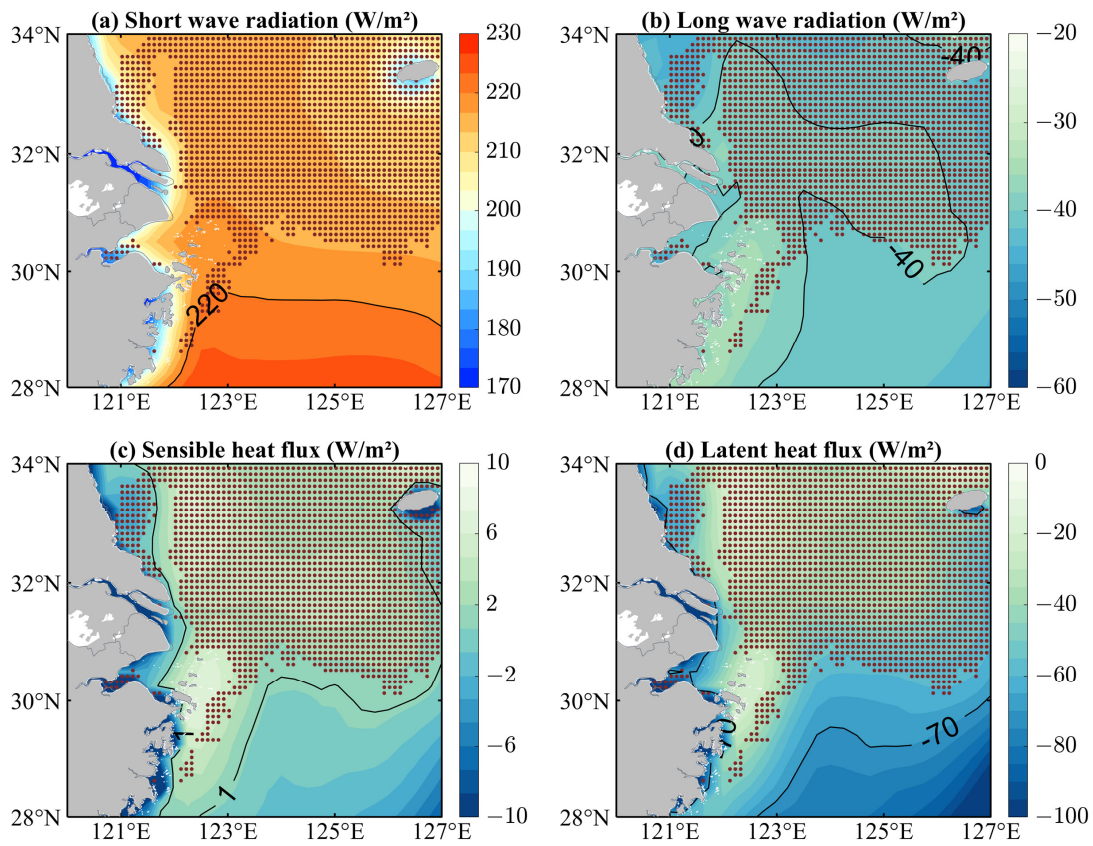


Figure 14. Spatial distribution of (a) SWRF, (b) LWRF, (c) SHF, and (d) LHF in the CRES throughout the summer of 1982–2021, and the red dots represent the mean intensity of MHWs in summer over 2 °C.

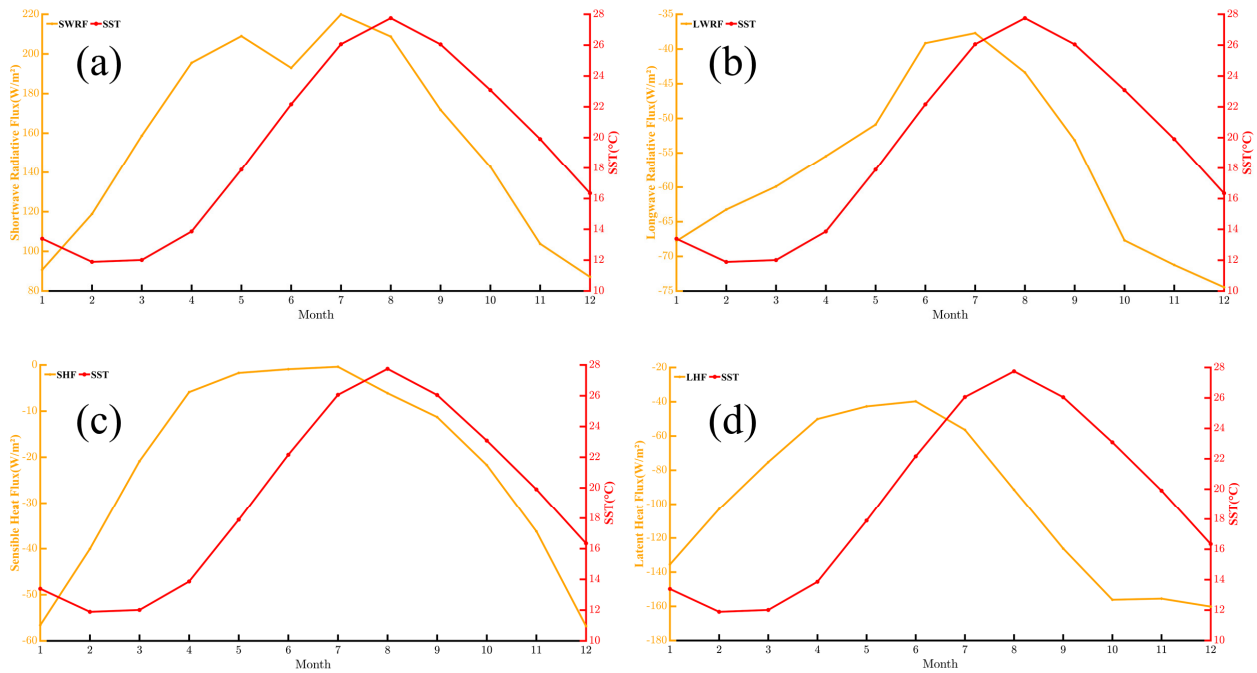


Figure 15. Monthly mean sea surface temperature and four radiation-flux time series from 1982 to 2021. (a) SWRF, (b) LWRF, (c) SHF, and (d) LHF. Radiation flux is represented by an orange line and sea surface temperature (units: °C) is represented by a red line.

4.2. Influence of Wind

Strong winds help to increase the mixing of upper ocean waters, bringing colder lower ocean waters to the surface and cooling of the upper ocean [25,46–49]. In order to delve deeper into the potential mechanisms of summer MHWs in the vicinity of the study area, this study analyzed mean 10 m wind speed spatial distribution characteristics during the summer months from 1982 to 2021. The regions with an average MHW intensity above 2 °C are highlighted in Figure 16. Figure 16 shows that, in 1982–2021, the average 10 m wind speed is approximately 3 m/s, decreasing from southeast to northwest. In particular, the coastal areas near Jeju Island show wind speeds below 2.5 m/s, and these areas correspond to the occurrence of MHWs with a higher mean intensity. Therefore, the occurrence of summer MHWs in the study area is closely related to the effect of strong winds on ocean–water mixing. Weak winds weaken the upper-layer mixing of seawater, allowing warm water to persist near the surface, providing favorable conditions for the summer MHW.

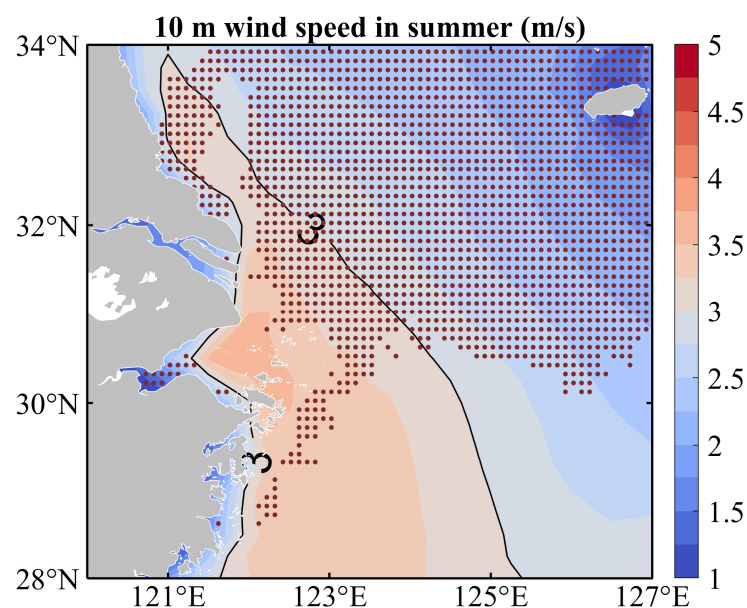


Figure 16. Spatial distribution of 10 m wind speed in the CRES during 1982–2021 in summer. The red dots represent the mean intensity of MHWs in summer over 2 °C.

4.3. Influence of El Niño

Extreme weather occurrences and modifications to the global meteorological system are frequently linked to strong El Niño events [21]. This meteorological phenomenon can trigger prolonged periods of high temperatures, creating favorable conditions for MHWs to occur. We have shown this trend by plotting the characteristic of the summer MHW intensity in 1982–2021 (as shown in Figure 17). Overall, before the year 2000, the occurrence of MHWs was relatively low (except for the years 1994 and 1998). However, after 2000, the summer MHW area increased significantly, accompanied by a rising pattern in the average MHW intensity. In 2016, the summer MHW intensity in the research area’s northern region exceeded 3.5 °C.

In addition, we performed a statistical analysis of the temporal variation in the number of grid points experiencing summer MHWs with an average intensity greater than 2 °C and the ONI (Oceanic Niño Index) in 1982–2021. As shown in Figure 18, the number of grid points experiencing MHWs generally shows an increasing trend. In strong El Niño years, the number of grid points was significantly higher than in other years, such as 1994, 1998, 2004, and 2016. These results indicate that intense El Niño events play a role in the incidence of MHWs.

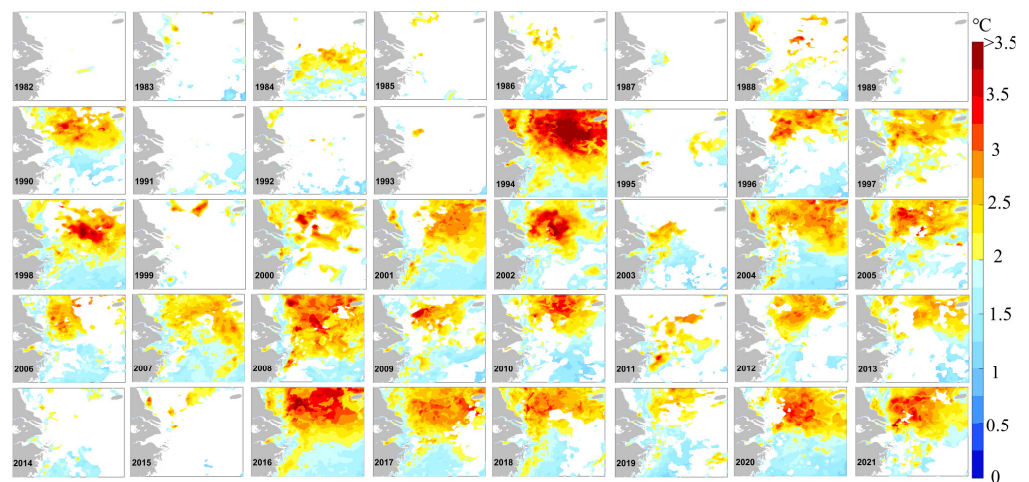


Figure 17. Spatial distribution of the summer MHW intensity in 1982–2021.

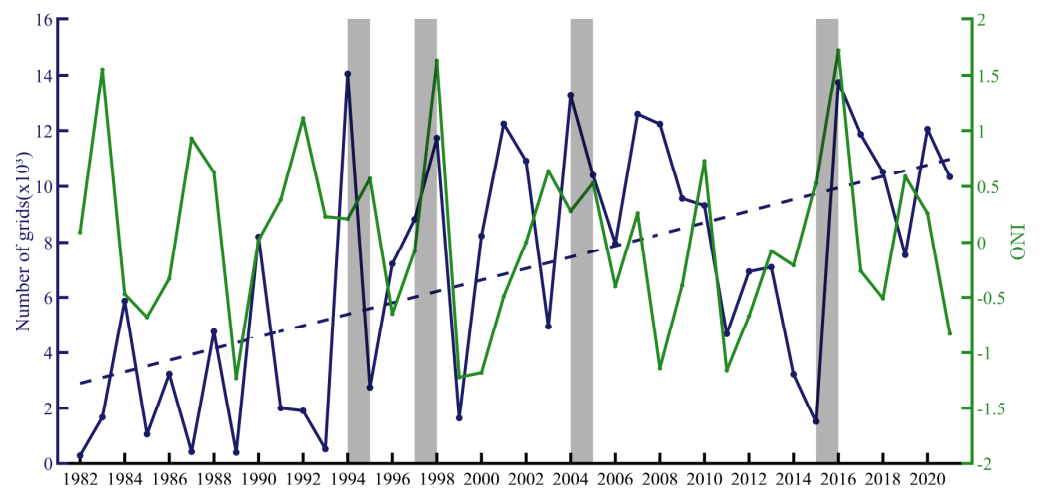


Figure 18. Time series of the grid points experiencing summer MHWs with an average intensity greater higher than 2 °C (blue line) and the Oceanic Niño Index (ONI) (green line) from 1982 to 2021. The gray shaded areas indicate periods of strong El Niño events.

This paper presents the spatial distribution of sea surface heat flux and 10 m wind speed from 9 October 2006 to 17 April 2007 and from 5 July to 1 August 1994, as shown in Figure 19. The aim is to provide a brief analysis of the possible factors contributing to the two special MHW events mentioned in Figure 2a,d, as well as to highlight the differences between causal factors. From Figure 19a,b, it can be observed that, at point A, the sea surface heat flux ranges from -50 W/m^2 to 50 W/m^2 , while the 10 m wind speed is below 1.5 m/s. Weak wind speed leads to less heat loss, allowing the extreme high-temperature state to persist for a longer period. Similarly, reduced vertical disturbances limit heat transfer from deeper ocean layers, further extending the duration of the MHW at point A, where the MHW duration lasted for 191 days from 9 October 2006 to 17 April 2007. Considering Figure 19c,d, it is evident that, at point B, despite the relatively high wind speed, around 4.5 m/s, the sea surface heat flux exceeds 200 W/m^2 . The larger sea surface heat flux, the ocean surface absorbs more solar radiation and retains heat more effectively. This leads to a higher temperature anomaly in the sea surface, exacerbating the intensity of the MHW at point B, where the average intensity of the MHW reached $4.93 \text{ }^\circ\text{C}$ from 5 July to 1 August 1994.

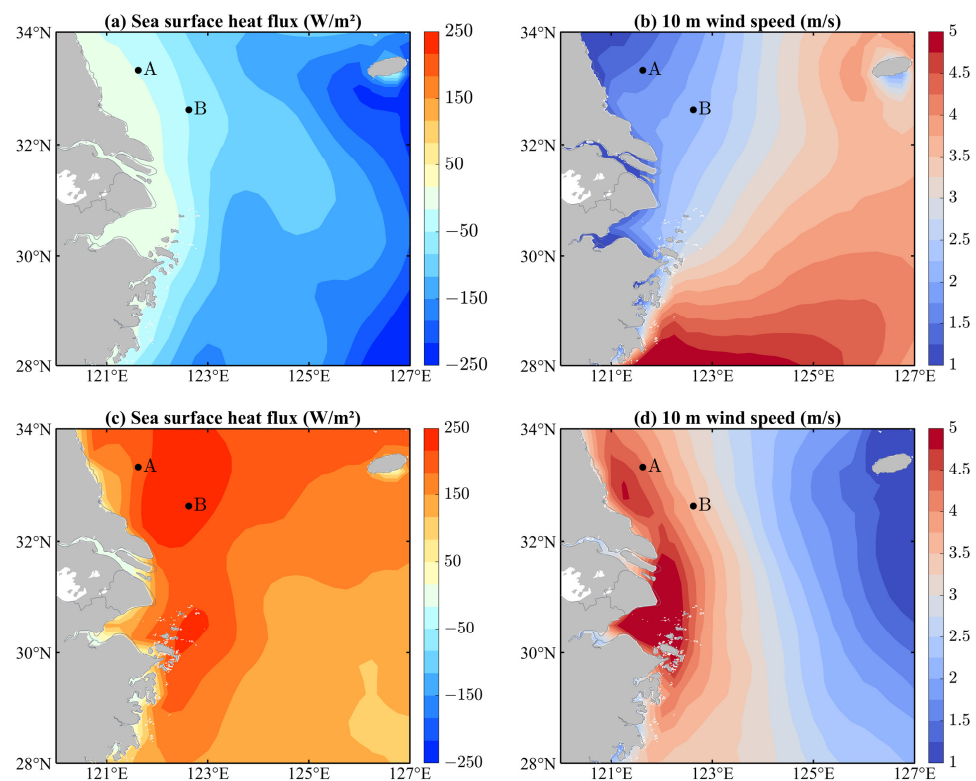


Figure 19. Spatial distribution of (a) mean sea surface heat flux and (b) 10 m wind speed from 9 October 2006 to 17 April 2007, and spatial distribution of (c) mean sea surface heat flux and (d) 10 m wind speed from 5 July to 1 August 1994. A and B are two points where typical MHWs occurred.

5. Conclusions

This paper analyzed the MHW's characteristics in the CRES in 1982–2021, with special emphasis on the variations during the summer season. The potential forcing mechanisms for the summer and the two specific MHWs were also briefly investigated. The main conclusions are summarized below:

1. Two severe MHW events were recorded in the study area. The first event occurred from 9 October 2006 to 17 April 2007 at the geographical coordinates of 124.225° E, 33.375° N. The second took place from 5 July to 1 August 1994 at the coordinates of 124.425° E, 32.125° N, with an average intensity of 4.93° C;
2. From 1982 to 2021, MHWs were significantly more frequent and intense along the coasts of Jiangsu, Shanghai, and Zhejiang. Moreover, key indicators of MHWs in the study area showed statistical significance ($p > 0.01$) in most marine regions. At the same time, there was an increasing trend in the total days (3.5 days/decade), duration (0.4 days/decade), and frequency (0.15 times/decade) of MHWs throughout the entire year. And the four indices showed a strong correlation with the annual mean sea surface temperature;
3. Various indicators of MHWs during the summer season from 1982 to 2021 exceeded those of other seasons. The spatial distribution of these indicators closely resembled the overall MHW's characteristics throughout the entire year, with relatively indistinct changing trends. The summer MHW's total days and frequency along the Jiangsu coast showed a trend value within the range of 0.4° C/10 years ($p > 0.05$);
4. During the summer season, the occurrence of MHWs was facilitated by the influence of the subtropical high-voltage system. Under its control, cloud cover decreased, leading to increased solar radiation. Additionally, the weaker wind speeds contributed to a decrease in ocean heat loss. These combined factors created favorable conditions

for the occurrence of summer MHWs. Simultaneously, powerful El Niño events contributed to some extent to the increased summer MHW intensity.

- Event A was primarily driven by weak wind speeds, while event B was predominantly influenced by the large sea surface heat flux. Despite their proximity, the characteristics of MHWs can vary significantly between these events, owing to the complex underlying mechanisms.

The MHW events will continue to increase, with major impacts on marine ecosystems, threats to the structure and function of marine organisms, as well as serious sociopolitical and economic consequences [50–52]. This study shows that the total days are increasing year by year in the research area, and the frequency of MHWs is becoming more severe, so it is especially crucial to thoroughly research MHW driving mechanisms in depth and to establish an emergency warning system for MHWs.

Author Contributions: Conceptualization, Q.J. and M.X.; methodology, M.X.; software, Q.J. and M.X.; validation, Q.J. and M.X.; formal analysis, M.X. and Q.Z.; investigation, M.X. and Z.M.; resources, Q.J.; data curation, M.X., Y.W. and M.G.; writing—original draft preparation, Q.J. and M.X.; writing—review and editing, Q.J.; visualization, M.X.; supervision, Q.J.; project administration, Q.J.; funding acquisition, Q.J. All authors have read and agreed to the published version of the manuscript.

Funding: This study was supported by the National Natural Science Foundation of China (41806004) and the National College Student Innovation and Entrepreneurship Training Program of China (202210340008).

Institutional Review Board Statement: Not applicable.

Informed Consent Statement: Not applicable.

Data Availability Statement: The SST data are available at https://data.marine.copernicus.eu/product/SST_GLO_SST_L4_REP_OBSERVATIONS_010_011/services, accessed on 26 May 2023. The ERA5 data are available at <https://cds.climate.copernicus.eu/cdsapp#!/search?type=dataset>, accessed on 28 May 2023. The Oceanic Niño Index are available at https://origin.cpc.ncep.noaa.gov/products/analysis_monitoring/ensostuff/ONI_v5.php, accessed on 10 July 2023.

Conflicts of Interest: The authors declare no conflicts of interest.

References

- Hobday, A.J.; Alexander, L.V.; Perkins, S.E.; Smale, D.A.; Straub, S.C.; Oliver, E.C.J.; Benthuyzen, J.A.; Burrows, M.T.; Donat, M.G.; Peng, M.; et al. A hierarchical approach to defining marine heatwaves. *Prog. Oceanogr.* **2016**, *141*, 227–238. [CrossRef]
- Olita, A.; Sorgente, R.; Natale, S.; Gaberšek, S.; Ribotti, A.; Bonanno, A.; Patti, B. Effects of the 2003 European heatwave on the Central Mediterranean Sea: Surface fluxes and the dynamical response. *Ocean Sci.* **2007**, *3*, 273–289. [CrossRef]
- Rosenzweig, C.; Karoly, D.; Vicarelli, M.; Neofotis, P.; Wu, Q.; Casassa, G.; Menzel, A.; Root, T.L.; Estrella, N.; Seguin, B.; et al. Attributing physical and biological impacts to anthropogenic climate change. *Nature* **2008**, *453*, 353–357. [CrossRef] [PubMed]
- Garrabou, J.; Coma, R.; Bensoussan, N.; Bally, M.; Chevaldonné, P.; Cigliano, M.; Diaz, D.; Harmelin, J.G.; Gambi, M.C.; Kersting, D.K.; et al. Mass mortality in Northwestern Mediterranean rocky benthic communities: Effects of the 2003 heat wave. *Glob. Change Biol.* **2009**, *15*, 1090–1103. [CrossRef]
- Feng, Y.T.; Bethel, B.J.; Dong, C.M.; Zhao, H.; Yao, Y.L.; Yu, Y. Marine heatwave events near Weizhou Island, Beibu Gulf in 2020 and their possible relations to coral bleaching. *Sci. Total Environ.* **2022**, *823*, 153414. [CrossRef] [PubMed]
- Smith, K.E.; Burrows, M.T.; Hobday, A.J.; King, N.G.; Moore, P.J.; Sen Gupta, A.; Thomsen, M.S.; Wernberg, T.; Smale, D.A. Biological Impacts of Marine Heatwaves. *Annu. Rev. Mar. Sci.* **2023**, *15*, 119–145. [CrossRef]
- Babcock, R.C.; Bustamante, R.H.; Fulton, E.A.; Fulton, D.J.; Haywood, M.D.E.; Hobday, A.J.; Kenyon, R.; Matear, R.J.; Plagányi, E.E.; Richardson, A.J.; et al. Severe Continental-Scale Impacts of Climate Change Are Happening Now: Extreme Climate Events Impact Marine Habitat Forming Communities along 45% of Australia’s Coast. *Front. Mar. Sci.* **2019**, *6*, 466674. [CrossRef]
- Smale, D.A.; Wernberg, T.; Oliver, E.C.J.; Thomsen, M.; Harvey, B.P.; Straub, S.C.; Burrows, M.T.; Alexander, L.V.; Benthuyzen, J.A.; Donat, M.G.; et al. Marine heatwaves threaten global biodiversity and the provision of ecosystem services. *Nat. Clim. Change* **2019**, *9*, 306–312. [CrossRef]
- Galli, G.; Solidoro, C.; Lovato, T. Marine Heat Waves Hazard 3D Maps and the Risk for Low Motility Organisms in a Warming Mediterranean Sea. *Front. Mar. Sci.* **2017**, *4*, 136. [CrossRef]
- Benthuyzen, J.; Feng, M.; Zhong, L.J. Spatial patterns of warming off Western Australia during the 2011 Ningaloo Niño: Quantifying impacts of remote and local forcing. *Cont. Shelf Res.* **2014**, *91*, 232–246. [CrossRef]

11. Wernberg, T.; Smale, D.A.; Tuya, F.; Thomsen, M.S.; Langlois, T.J.; Bettignies, T.; Bennett, S.; Rousseaux, C.S. An extreme climatic event alters marine ecosystem structure in a global biodiversity hotspot. *Nat. Clim. Change* **2012**, *3*, 78–82. [[CrossRef](#)]
12. Mills, K.; Pershing, A.; Brown, C.; Chen, Y.; Chiang, F.S.; Holland, D.; Lehuta, S.; Nye, J.; Sun, J.; Thomas, A.; et al. Fisheries Management in a Changing Climate: Lessons from the 2012 Ocean Heat Wave in the Northwest Atlantic. *Oceanography* **2013**, *26*, 191–195. [[CrossRef](#)]
13. Conti, S.; Meli, P.; Minelli, G.; Solimini, R.; Toccaceli, V.; Vichi, M.; Beltrano, C.; Perini, L. Epidemiologic study of mortality during the Summer 2003 heat wave in Italy. *Environ. Res.* **2005**, *98*, 390–399. [[CrossRef](#)]
14. Benthuyesen, J.A.; Oliver, E.C.J.; Feng, M.; Marshall, A.G. Extreme Marine Warming across Tropical Australia during Austral Summer 2015–2016. *J. Geophys. Res. Ocean.* **2018**, *123*, 1301–1326. [[CrossRef](#)]
15. Kajtar, J.B.; Bachman, S.D.; Holbrook, N.J.; Pilo, G.S. Drivers, Dynamics, and Persistence of the 2017/2018 Tasman Sea Marine Heatwave. *J. Geophys. Res. Ocean.* **2022**, *127*, e2022JC018931. [[CrossRef](#)]
16. Oliver, E.C.J.; Benthuyesen, J.A.; Bindoff, N.L.; Hobday, A.J.; Holbrook, N.J.; Mundy, C.N.; Perkins-Kirkpatrick, S.E. The unprecedented 2015/16 Tasman Sea marine heatwave. *Nat. Commun.* **2017**, *8*, 16101. [[CrossRef](#)] [[PubMed](#)]
17. Trenberth, K.E. Framing the way to relate climate extremes to climate change. *Clim. Change* **2012**, *115*, 283–290. [[CrossRef](#)]
18. Wu, L.; Cai, W.; Zhang, L.; Nakamura, H.; Timmermann, A.; Joyce, T.; McPhaden, M.J.; Alexander, M.; Qiu, B.; Visbeck, M.; et al. Enhanced warming over the global subtropical western boundary currents. *Nat. Clim. Change* **2012**, *2*, 161–166. [[CrossRef](#)]
19. Holbrook, N.; Scannell, H.; Sen Gupta, A.; Benthuyesen, J.; Feng, M.; Oliver, E.; Alexander, L.; Burrow, M.; Donat, M.; Hobday, A. A global assessment of marine heatwaves and their drivers. *Nat. Commun.* **2019**, *10*, 2624. [[CrossRef](#)]
20. Oliver, E.C.J.; Benthuyesen, J.A.; Darmaraki, S.; Donat, M.G.; Hobday, A.J.; Holbrook, N.J.; Schlegel, R.W.; Sen Gupta, A. Marine Heatwaves. *Annu. Rev. Mar. Sci.* **2021**, *13*, 313–342. [[CrossRef](#)]
21. Carrasco, D.; Pizarro, O.; Jacques-Coper, M.; Narváez, D.A. Main drivers of marine heat waves in the eastern South Pacific. *Front. Mar. Sci.* **2023**, *10*, 1129276. [[CrossRef](#)]
22. Lee, H.; Calvin, K.; Dasgupta, D.; Krinner, G.; Mukherji, A.; Thorne, P.W.; Trisos, C.; Romero, J.; Aldunce, P.; Barrett, K.; et al. *Climate Change 2023: Synthesis Report. Contribution of Working Groups I, II and III to the Sixth Assessment Report of the Intergovernmental Panel on Climate Change*; IPCC: Geneva, Switzerland, 2023; pp. 35–115. [[CrossRef](#)]
23. Frölicher, T.L.; Fischer, E.M.; Gruber, N. Marine heatwaves under global warming. *Nature* **2018**, *560*, 360–364. [[CrossRef](#)] [[PubMed](#)]
24. Mora, C.; Spirandelli, D.; Franklin, E.C.; Lynham, J.; Kantar, M.B.; Miles, W.; Smith, C.Z.; Freel, K.; Moy, J.; Louis, L.V.; et al. Broad threat to humanity from cumulative climate hazards intensified by greenhouse gas emissions. *Nat. Clim. Change* **2018**, *8*, 1062–1071. [[CrossRef](#)]
25. Yao, Y.L.; Wang, C.Z. Variations in Summer Marine Heatwaves in the South China Sea. *J. Geophys. Res. Ocean.* **2021**, *126*, e2021JC017792. [[CrossRef](#)]
26. Miao, Y.; Xu, H.; Liu, J. Variation of summer marine heatwaves in the Northwest Pacific and associated air-sea interaction. *J. Trop. Oceanogr.* **2021**, *40*, 31–43.
27. Kuroda, H.; Setou, T. Extensive Marine Heatwaves at the Sea Surface in the Northwestern Pacific Ocean in Summer 2021. *Remote Sens.* **2021**, *13*, 3989. [[CrossRef](#)]
28. Chen, S.J.; Yao, Y.L.; Feng, Y.T.; Zhang, Y.C.; Xia, C.S.; Sian, K.T.C.L.K.; Dong, C.M. Characteristics and Drivers of Marine Heatwaves in 2021 Summer in East Korea Bay, Japan/East Sea. *Remote Sens.* **2023**, *15*, 713. [[CrossRef](#)]
29. Cheng, L.; Trenberth, K.; Fasullo, J.; Boyer, T.; Abraham, J.; Zhu, J. Improved estimates of ocean heat content from 1960 to 2015. *Sci. Adv.* **2017**, *3*, e1601545. [[CrossRef](#)] [[PubMed](#)]
30. Yao, Y.L.; Wang, C.Z. Marine heatwaves and cold-spells in global coral reef zones. *Prog. Oceanogr.* **2022**, *209*, 102920. [[CrossRef](#)]
31. Liu, S.; Lao, Q.; Zhou, X.; Jin, G.; Chen, C.; Chen, F. Impacts of Marine Heatwave Events on Three Distinct Upwelling Systems and Their Implications for Marine Ecosystems in the Northwestern South China Sea. *Remote Sens.* **2024**, *16*, 131. [[CrossRef](#)]
32. Wang, A.; Wang, H.; Fan, W.; Luo, J.; Li, W.; Xu, S. Study on characteristics of marine heatwave in the China offshore in 2019. *Haiyang Xuebao* **2021**, *43*, 35–44.
33. Cai, R.; Tan, H.; Qi, Q. Impacts of and adaptation to inter-decadal marine climate change in coastal China seas. *Int. J. Climatol.* **2016**, *36*, 3770–3780. [[CrossRef](#)]
34. Zhang, W.; Zheng, Z.; Zhang, T.; Chen, T.J.H.X. Strengthened marine heatwaves over the Beibu Gulf coral reef regions from 1960 to 2017. *Haiyang Xuebao* **2020**, *42*, 45–52.
35. Wang, Q.; Li, Q.; Li, Y.; Liu, Y.; Wang, Y.J.H. Temporal and spatial characteristics of marine heat waves in the Bohai Sea and Yellow Sea during 1982–2019. *Haiyang Xuebao* **2021**, *43*, 38–49.
36. Meehl, G.A.; Tebaldi, C. More Intense, More Frequent, and Longer Lasting Heat Waves in the 21st Century. *Science* **2004**, *305*, 994–997. [[CrossRef](#)] [[PubMed](#)]
37. Cronin, M.F.; Kwon, Y.-O.; Joyce, T.M.; Qiu, B.; Samelson, R.M.; Small, R.J.; Kelly, K.A. Western Boundary Currents and Frontal Air–Sea Interaction: Gulf Stream and Kuroshio Extension. *J. Clim.* **2010**, *23*, 5644–5667. [[CrossRef](#)]
38. Yao, Y.L.; Wang, J.J.; Yin, J.J.; Zou, X.Q. Marine Heatwaves in China’s Marginal Seas and Adjacent Offshore Waters: Past, Present, and Future. *J. Geophys. Res. Ocean.* **2020**, *125*, e2019JC015801. [[CrossRef](#)]
39. Gao, G.D.; Marin, M.; Feng, M.; Yin, B.S.; Yang, D.Z.; Feng, X.R.; Ding, Y.; Song, D.H. Drivers of Marine Heatwaves in the East China Sea and the South Yellow Sea in Three Consecutive Summers during 2016–2018. *J. Geophys. Res. Ocean.* **2020**, *125*, e2020JC016518. [[CrossRef](#)]

40. Tan, H.; Cai, R. What caused the record-breaking warming in East China Seas during August 2016? *Atmos. Sci. Lett.* **2018**, *19*, e853. [[CrossRef](#)]
41. Mohamed, B.; Nagy, H.; Ibrahim, O. Spatiotemporal Variability and Trends of Marine Heat Waves in the Red Sea over 38 Years. *J. Mar. Sci. Eng.* **2021**, *9*, 842. [[CrossRef](#)]
42. Chen, X.; Zhou, T. Relative contributions of external SST forcing and internal atmospheric variability to July–August heat waves over the Changjiang River valley. *Clim. Dyn.* **2017**, *51*, 4403–4419. [[CrossRef](#)]
43. Wang, P.Y.; Tang, J.P.; Sun, X.G.; Wang, S.Y.; Wu, J.; Dong, X.N.; Fang, J. Heat Waves in China: Definitions, Leading Patterns, and Connections to Large-Scale Atmospheric Circulation and SSTs. *J. Geophys. Res. Atmos.* **2017**, *122*, 10679–10699. [[CrossRef](#)]
44. Hu, S.; Li, S. Progress and prospect of marine heatwave study. *Adv. Earth. Sci.* **2022**, *37*, 51–64. [[CrossRef](#)]
45. Wang, Q.; Zhang, B.; Zeng, L.L.; He, Y.K.; Wu, Z.W.; Chen, J. Properties and Drivers of Marine Heat Waves in the Northern South China Sea. *J. Phys. Oceanogr.* **2022**, *52*, 917–927. [[CrossRef](#)]
46. Amaya, D.J.; Miller, A.J.; Xie, S.P.; Kosaka, Y. Physical drivers of the summer 2019 North Pacific marine heatwave. *Nat. Commun.* **2020**, *11*, 1903. [[CrossRef](#)] [[PubMed](#)]
47. Schlegel, R.W.; Oliver, E.C.J.; Chen, K. Drivers of Marine Heatwaves in the Northwest Atlantic: The Role of Air–Sea Interaction During Onset and Decline. *Front. Mar. Sci.* **2021**, *8*, 627970. [[CrossRef](#)]
48. Chiswell, S.M. Atmospheric wavenumber-4 driven South Pacific marine heat waves and marine cool spells. *Nat. Commun.* **2021**, *12*, 4779. [[CrossRef](#)]
49. Gentemann, C.L.; Fewings, M.R.; García-Reyes, M. Satellite sea surface temperatures along the West Coast of the United States during the 2014–2016 northeast Pacific marine heat wave. *Geophys. Res. Lett.* **2017**, *44*, 312–319. [[CrossRef](#)]
50. Oliver, E.C.J.; Burrows, M.T.; Donat, M.G.; Sen Gupta, A.; Alexander, L.V.; Perkins-Kirkpatrick, S.E.; Benthuisen, J.A.; Hobday, A.J.; Holbrook, N.J.; Moore, P.J.; et al. Projected Marine Heatwaves in the 21st Century and the Potential for Ecological Impact. *Front. Mar. Sci.* **2019**, *6*, 734. [[CrossRef](#)]
51. Androulidakis, Y.S.; Krestenitis, Y.N. Sea Surface Temperature Variability and Marine Heat Waves over the Aegean, Ionian, and Cretan Seas from 2008–2021. *J. Mar. Sci. Eng.* **2022**, *10*, 42. [[CrossRef](#)]
52. Marullo, S.; Serva, F.; Iacono, R.; Napolitano, E.; di Sarra, A.; Meloni, D.; Monteleone, F.; Sferlazzo, D.; De Silvestri, L.; de Toma, V.; et al. Record-breaking persistence of the 2022/23 marine heatwave in the Mediterranean Sea. *Environ. Res. Lett.* **2023**, *18*, 114041. [[CrossRef](#)]

Disclaimer/Publisher’s Note: The statements, opinions and data contained in all publications are solely those of the individual author(s) and contributor(s) and not of MDPI and/or the editor(s). MDPI and/or the editor(s) disclaim responsibility for any injury to people or property resulting from any ideas, methods, instructions or products referred to in the content.